

# Memoryless self-reinforcing directionality in endosomal active transport within living cells

Kejia Chen<sup>1</sup>, Bo Wang<sup>2,3\*†</sup> and Steve Granick<sup>1,2,4,5,6\*</sup>

**In contrast to Brownian transport, the active motility of microbes, cells, animals and even humans often follows another random process known as truncated Lévy walk<sup>1,2</sup>. These stochastic motions are characterized by clustered small steps and intermittent longer jumps that often extend towards the size of the entire system. As there are repeated suggestions, although disagreement, that Lévy walks have functional advantages over Brownian motion in random searching and transport kinetics<sup>3–8</sup>, their intentional engineering into active materials could be useful. Here, we show experimentally in the classic active matter system of intracellular trafficking<sup>9–15</sup> that Brownian-like steps self-organize into truncated Lévy walks through an apparent time-independent positive feedback such that directional persistence increases with the distance travelled persistently. A molecular model that allows the maximum output of the active propelling forces to fluctuate slowly fits the experiments quantitatively. Our findings offer design principles for programming efficient transport in active materials.**

With obvious differences in their trajectories Brownian motion and a Lévy walk are composed of, respectively, exponentially distributed steps and steps drawn from probability distributions with heavy power-law tails<sup>1,2</sup> (Fig. 1). In almost all physical systems the power-law tail of Lévy walks is inevitably cut off, or truncated, at a characteristic scale that often is the system size. Brownian and truncated Lévy transport (for brevity, ‘truncated’ will be omitted for the rest of this paper) have been studied extensively in separate physical systems, and have been viewed as distinct transport mechanisms that arise from different origins and that have different functions<sup>1–7</sup>. Paradoxically, mathematical analysis casts doubt on this distinction, as exponentially distributed independent variables can sum into power-law distributions provided there are proper correlations or ‘memory’<sup>216,17</sup>, but a great difficulty can be to find the physical justification for such formalism. In this paper, in a system lacking memory, we present experiments and a simple molecular-based mechanism showing that self-reinforcing directionality can be programmed in a generalizable and physically realistic way that allows Lévy transport over long distances to arise from local Brownian-like motions.

Our field of application concerns self-propelled objects known as ‘active matter’<sup>9–15</sup>. We consider a classic system of active transport, endosomal transport in cells<sup>18–22</sup>. Mathematically, illustrated schematically in Fig. 1, Brownian random walkers can convert to Lévy walks when the probability  $p(L)$  of travelling in some direction grows with the distance already travelled<sup>16,17</sup>. On the

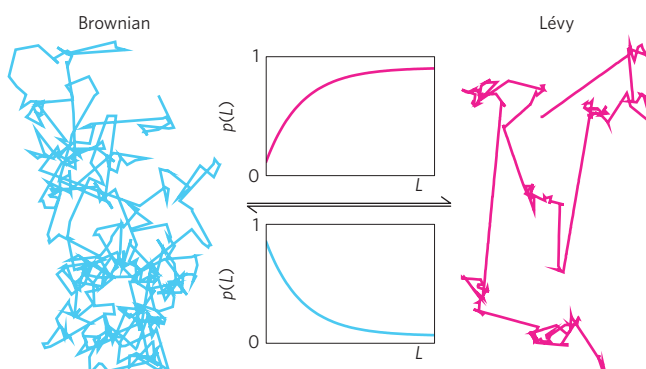


**Figure 1 | Feedback in directional persistence transforms transport dynamics.** Exponentially distributed steps of Brownian motion (left) self-organize into power-law distributed flights of truncated Lévy walk (right) under the action of positive feedback in directional persistence. Contrariwise, negative feedback reverses this.

other hand, how can directional persistence with positive feedback be programmed, if any long-term memory is expected to be disrupted by frequent random noises? Figure 2 shows the physical idea. Cargo (endosome) is dragged by multiple molecular motors along straight microtubule tracks processively, but during this process some motors may detach from the microtubule and rebind stochastically on a timescale shorter than 1 s. An opposing force, a combination of viscous drag and viscoelastic constraints, is shared equally between engaged motors bound to the microtubule<sup>11,20–22</sup>. When the force on each motor (‘load’) exceeds the stall force, transport pauses. Thus, this active transport consists of sequences of motion, separated by pauses: it is a catenation of hundreds of unidirectional molecular steps, called a ‘run’, whose direction is determined by the orientation of microtubules and the polarity of motors. Although these transient unidirectional motions have been extensively studied from certain points of view<sup>18,19</sup>, the directional correlations between adjacent runs on larger length scales have not been considered previously. As microtubules are so stiff that they are straight on the scale of hundreds of micrometres, we suppose that transport turns only when all engaged motors dissociate from one microtubule and then attach to another nearby microtubule pointing in a different direction<sup>10,23</sup>. Indeed, strands of microtubule are known to cross paths intermittently at spacings ( $\sim 1\ \mu\text{m}$  for the mammalian epithelium cells used in this study<sup>24</sup>) smaller than or comparable to the motor processive distance (0.5–5  $\mu\text{m}$ ; ref. 21). In

<sup>1</sup>Department of Chemical and Biomolecular Engineering, University of Illinois, Urbana, Illinois 61801, USA. <sup>2</sup>Department of Materials Science, University of Illinois, Urbana, Illinois 61801, USA. <sup>3</sup>Institute for Genomic Biology, University of Illinois, Urbana, Illinois 61801, USA. <sup>4</sup>Department of Chemistry, University of Illinois, Urbana, Illinois 61801, USA. <sup>5</sup>Department of Physics, University of Illinois, Urbana, Illinois 61801, USA. <sup>6</sup>IBS Center for Soft and Living Matter, UNIST, Ulsan 689-798, South Korea. <sup>†</sup>Present address: Department of Bioengineering, Stanford University, Stanford, California 94305, USA.

\*e-mail: wangbo@stanford.edu; sgranick@ibs.re.kr

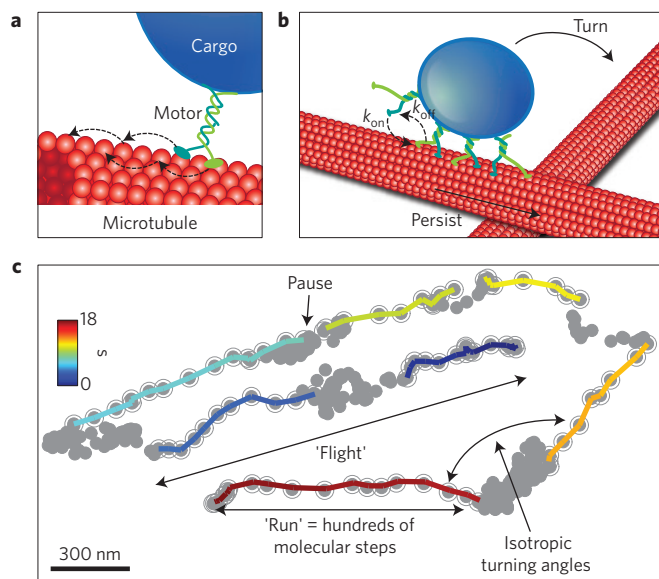


**Figure 2 | Trajectories of endosomes in live cells.** **a**, Cargo is transported along microtubules dragged by molecular motors with nanometre-sized steps. The motors can pause, dissociate and rebind. **b**, Microtubules extend in multiple directions and cross paths to form networks, leading to complexity in transport directionality, especially when multiple motors bind simultaneously to work as a team. **c**, A representative trajectory with runs, turns and flights. See text for definitions. Grey dots are the tracked positions of the trajectory, and the active portions detected by wavelet analysis are highlighted by circles. The lines with colour denote elapsed time with scale shown in the inset.

linking this physical situation mechanistically to the mathematical idea illustrated in Fig. 1, we reasoned that because motors dissociate exponentially more slowly as load decreases<sup>20–22</sup>, as more motors on an endosome bind to the same microtubule to share the load, dissociation happens more slowly. Consequently, dissociated motors have more time to rebind, and hence cargo transport should continue farther along that microtubule.

Testing this idea, we used fluorescence imaging and single-particle tracking<sup>11</sup> to collect data about hundreds of thousands of runs in live mammalian cells, as described in Methods and Supplementary Information. Each run lasted  $\sim 1$  s in time and  $\sim 0.5 \mu\text{m}$  in distance on average, and concerned two types of endosome, tagged by fluorescently labelled epidermal growth factor (EGF) and low-density lipoprotein (LDL) in parallel sets of experiments. To minimize potential photo-toxicity, each cell was observed for  $\sim 10$  min. To avoid conceivable artefacts from the two-dimensional projection of the motions, and to accurately locate the centres (spatial precision  $< 5$  nm and temporal resolution 50 ms; ref. 11), we employed laminated optical imaging with an optical sheet  $\sim 1 \mu\text{m}$  thick (Supplementary Information). To separate active runs from local jiggling, a wavelet-based method was employed<sup>25</sup>, enabling automated determination of active runs from over 100 million tracked positions. Supplementary Movies 1 and 2 illustrate the high quality of the data.

Trajectories that we observed are illustrated in Fig. 2c, and more in Supplementary Fig. 1. Appearing random to the eye, they are consistent with random walks reported in other recent studies<sup>14,15</sup>; however, separating the runs from the local jiggling reveals the unusual nature of the randomness. We observe a high tendency for transport to maintain directionality between runs before turns (Fig. 3a), consistent with what has been observed in the literature<sup>26,27</sup>. When analysed statistically, the average probability to switch direction after each run was  $\sim 0.25$ . Focusing on the

actual turns, we defined ‘flights’, which are consecutive runs that persist in direction punctuated by pauses (Fig. 2c), and identified the turning points between flights, employing to do so the error-radius analysis standard in the field of ecology<sup>7</sup> (Methods and Supplementary Figs 2 and 3). We find that the turns were made in isotropic directions (Fig. 3a), which implies no preferred direction in our experimental time window ( $\sim 10$  min). Importantly, isotropy is a necessary condition for either Brownian or Lévy walks<sup>5,7</sup>. This new analysis reveals that  $p(L)$  grew with  $L$ , as illustrated in Fig. 3b, suggesting that this system conforms to the Brownian-to-Lévy scenario shown in Fig. 1.

Extending the analysis, we identify in the data power-law tails of flight-length distributions that are clearly different from commonplace Brownian random walks, whose step-size distribution is exponential. In Fig. 3c, the plot of relative probability against distance on log-log scales confirms that exponential events of individual run lengths added up to a power-law tail of flight-length distribution, with a power-law slope of  $\mu = -2$ , determined from maximum likelihood estimation. The range of the power-law tail does not depend on how the data are binned to calculate the distributions (Fig. 3c, inset). It spans the entire length scale that is physically reasonable: from the smallest possible step size, which is the individual run length, to the largest possible step size, which is the size of the cells. Indeed, in other systems, power-law tails with a slope of  $-2$  have been identified as advantageous in random searching, although there is heated argument on this matter<sup>3,4</sup>. The coexistence of self-reinforcing persistence and the transition from exponential to power-law step distributions in this experimental data set is consistent with the mathematical guideline sketched in Fig. 1.

As the coexistence of exponentially distributed steps and power-law distributed flights is so non-standard for other random walks that experimentalists have measured, we tested these relations using Akaike’s information criterion for the discrimination between models<sup>28</sup>. The merit of this analysis is to evaluate the raw data points directly, circumventing model-dependent interpretation. For run length, an exponential tail is favoured with a relative likelihood (the Akaike weight) of 1, and for turn-to-turn flight length, a power-law is favoured with a weight of 1. The unusual Akaike weight of unity emerges because our large data sets allow unambiguous selection of the more likely model (Methods).

But what molecular mechanism might underpin this? Although in classic random-walk models it is common to introduce memory kernels to describe such dynamic patterns, the required memory over long time and large length scales lacks obvious reasonable grounding in biology. To rule out the obvious variables, we varied the cell type (HeLa and DU145 cells), and the cargo types (EGF- and LDL-containing endosomes), which are known to be transported by different sets of motor proteins through separate pathways. As the fluctuations of surrounding cytoskeleton (mainly actin networks) have been indicated to contribute to the transport directionality<sup>14,15</sup>, we treated the cells pharmacologically with latrunculin A (LatA), which completely disrupts the actin networks. The directional persistence and the nature of the length distributions were invariant under all of these conditions (Fig. 3d). This was so even when we directly perturbed the motor-microtubule interactions: for example, overexpressed microtubule-associated protein 4 (MAP4) forms road blocks on microtubules, and trichostatin A (TSA) enhances the motor processivity by inducing microtubule acetylation (Supplementary Figs 4 and 5). Indeed, despite minor differences in the directional persistence (Fig. 3b), all of the flight-length distributions collapse (Fig. 3d).

To explain the observed self-reinforcing directionality without introducing memory, we develop a model that builds on a transient-rate model used widely to describe intracellular transport<sup>20</sup>. We assume that only motors attached to cargo in the vicinity of the microtubule are available to bind to it<sup>29</sup>, and that this pool of avail-

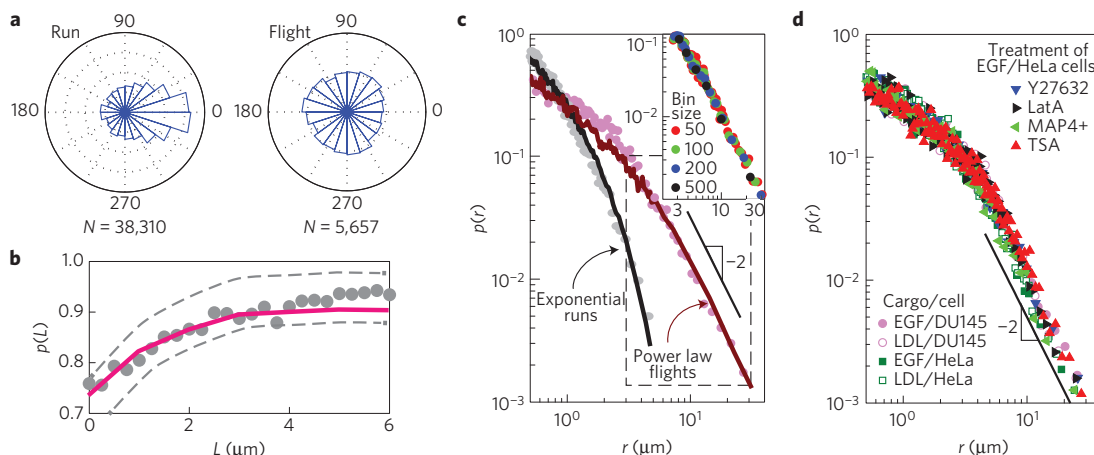


**Figure 3 | Combined experiments and numerical modelling show that positive feedback in directional persistence during intracellular trafficking transforms Brownian-like steps to truncated Lévy walks.** **a**, Distributions of angles between consecutive runs and flights. Note that unlike runs, which are statistically directional, the flights are statistically isotropic. Data are from ~40,000 runs of EGF-containing endosomes in DU145 cells. **b**, Positive feedback during walks along microtubules: persistence probability  $p$  is plotted against accumulated curvilinear distance travelled in that direction,  $L$ . Symbols are from the data of EGF-containing endosomes in DU145 cells. Dashed lines show the bounds between which the curves from all eight experimental conditions reside, as specified below. **c**, Log-log plot of relative probability against distance showing that exponential and power-law statistics describe individual run length and turn-to-turn flight length, respectively, for EGF-containing endosomes in DU145 cells. The range of the power-law tail, determined by a goodness-of-fit test, is highlighted by the dashed rectangle. Inset: Power-law tail is independent of the bin size, with the number of data points per bin indicated in the plot. The line with slope  $-2$  shows the maximum likelihood estimation of the power-law tail. In **b, c**, lines through the data are drawn from the model, with parameters summarized in Supplementary Table 1; the model produces good fits over the full distributions, not just in the tails. **d**, Flight-length distributions for eight different experimental conditions collapse on a master curve. Cargos and cells: EGF (or LDL)/DU145 (or HeLa) means EGF- (or LDL)-containing endosomes in DU145 (or HeLa) cells; treatments: EGF-containing endosomes in HeLa cells treated as specified in Methods with Y-27632, LatA and TSA, or with MAP4 overexpressed.

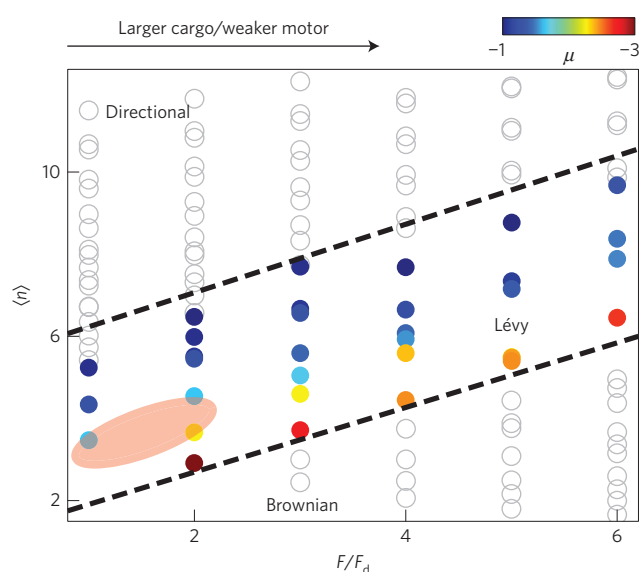


**Figure 4 | The balance of competing factors determines feedback and the nature of the transport dynamics.** The flight-length distribution from 210 sets of numerically simulated trajectories is summarized, with the reduced opposing force  $F/F_d$  on the abscissa and the average number of engaged motors  $\langle n \rangle$  on the ordinate. When a constructive factor dominates ( $\langle n \rangle$ ), transport is unidirectional; when a destructive factor dominates ( $F/F_d$ ), transport reverts to Brownian (open symbols); in between, a pattern of truncated Lévy walks emerges (filled symbols). Simulations that exhibit Lévy dynamics are colour-coded (upper right) to represent the exponent of the power-law tail. The parameter range that fits the experiments reported in this paper is highlighted with a shaded oval area, which concentrates at small values of  $F/F_d$ . This is consistent with the small sizes of the endosomes that lead to the small opposing forces.

able motors resets each time that all engaged motors dissociate and the transport restarts on another microtubule. This is reasonable, as the cargo may approach the microtubule in various different orientations, and the distribution of the motors on the cargo surface is expected to be heterogeneous<sup>29</sup>. Our numerical simulations based on this model, specified in Methods, reproduced quantitatively all of the most relevant experimental observations: positive feedback in directionality, exponential run-length distributions, and a power-law tail in flight-length distributions (Fig. 3, and more discussion in Supplementary Information). Thus, although this minimalistic model does not include high-order effects that have been implied to affect the probability of switching directions<sup>27</sup>, such as the inherent molecular mechanics of motors, motor-motor interactions and track geometry, it includes the most important necessary physics: the slow fluctuations of the number of available motors, which are further coupled nonlinearly to the fast motor-binding and unbinding events through the load-dependent unbinding rate. These ideas are sufficient to produce the effective positive feedback that constructs Lévy dynamics from Brownian steps.

To rationalize this intuitively, we walked through the parameter space that is physically realistic using numerical simulations (Fig. 4), and noticed that the parameter space can collapse onto a two-dimensional space: the average number of engaged motors,  $\langle n \rangle$ , and the opposing force normalized by the detachment force,  $F/F_d$  (Supplementary Fig. 6). Specifically,  $\langle n \rangle$  depends on the maximum number of the available motors on cargo, and the motor binding and unbinding rates (Methods); and  $F/F_d$  increases with bigger cargo, and decreases with stronger motors. Lévy dynamics emerges when the feedback reaches a right balance between these two opposing factors,  $\langle n \rangle$  as a constructive factor that encourages motion to maintain directional persistence, and  $F/F_d$  as a destructive factor that encourages the transport to change direction. When the constructive factor dominates, transport is unidirectional; when the destructive factor wins, transport reverts to Brownian; within a broad range in between, Lévy walk patterns emerge. This is



summarized in a plot of  $\langle n \rangle$  against reduced opposing force (Fig. 4). This reduced description explains why molecular details have only a marginal effect on our experiments, because contributions from molecular kinetics may cancel each other while the collective output is maintained. For example, as confirmed by simulations, a higher unbinding rate can be compensated by a higher number of motors that are available on the cargo surface, as long as the average number of engaged motors remains constant (Supplementary Fig. 6).

The phenomenon of memoryless self-reinforcing directional transport seems to be general, and can arise from other mechanistic models than the one developed here to describe the system that we happened to be studying. In principle, it can arise from abundant other kinds of system that likewise lack long-term memory: for example, transport driven by physical sensing of chemical gradients<sup>8</sup> and conceptual sensing of information<sup>30</sup>. The framework proposed in this paper has bearing on providing rules on how to programme non-Brownian transport in other active systems of interest to physicists and materials scientists.

## Methods

**Imaging and tracking.** Fluorescently labelled endosomes were imaged in live mammalian cells under physiological conditions. The labelling approaches were selected and optimized to satisfy two stringent criteria. First, we required specific labelling of organelles whose fate within the cell is known. Second, we required the labelling to be specific and to present bright and stable fluorescent spots with average organelle separation larger than 3  $\mu\text{m}$ , so as to allow position information to be extracted with high resolution below the optical diffraction limit. Trajectories were generated from movies with a frame rate of 50 ms. This was chosen to be longer than the molecular motor stepping time on microtubules ( $\sim 1$  ms) to filter out the expected molecular noise. More experimental details are provided in the Supplementary Information.

**Cell treatments.** To confirm that the observed endosomal mobility is active transport by motor proteins along microtubules, we disrupted the microtubules with nocodazole (5  $\mu\text{g ml}^{-1}$ ), and the mobility stalled as expected. To rule out the contribution by actin networks<sup>14,15</sup>, we disrupted actin networks with LatA (0.08  $\mu\text{g ml}^{-1}$ ), and no statistical change in terms of relative portions of persistent, turning, and tug-of-war events of endosomal mobility was observed (Supplementary Fig. 4). To perturb the overall cytoskeleton, 5  $\mu\text{M}$  TSA or 50  $\mu\text{M}$  Y-27632 was added 60 min or 30 min before imaging, respectively. Overexpression of MAP4 was achieved by transient transfection of MAP4 fused to emerald GFP (Invitrogen). Cells with bright green fluorescence, indicating MAP4 expression at a high level, were chosen for imaging. These perturbations induced changes in mean run time and transport speed as expected (Supplementary Fig. 5).

**Statistical analysis.** Active transport was determined using the multiscale wavelet transform described elsewhere<sup>25</sup>. To define turn-to-turn steps, we used the error-radius method documented in the literature<sup>7</sup>. This analysis was preferred to direct splitting of the intersection angles between runs, which is prohibitively sensitive to tracking noise especially when runs are short (Supplementary Fig. 1). Runs between two consecutive turning points are defined as persistent and they are lumped together into a single flight, with the flight length calculated as the sum of the run lengths. The relative abundance of runs that are persistent, turning, and reversing directions ('tug-of-war') was quantified (Supplementary Fig. 4). However, as tug-of-war events do not change the overall angle of the transport, we excluded them from subsequent analysis.

To calculate the run length and flight-length distributions, we used an equal number of data points per bin instead of an equal distance per bin that is known to give larger statistical errors in the tail because of the much smaller counts per bin in the tail. This binning method has been shown to reproduce the actual shape of distribution and avoid large uncertainty in fitting the tail. To distinguish exponential, stretched exponential, and power-law distributions, model selection was carried out following the standard literature method, Akaike information criterion<sup>28</sup>. Briefly, the log-likelihood functions for each model were computed as described in the literature with the range of the tails ( $>2.9 \mu\text{m}$ ) determined by the goodness-of-fit tests; and then the relative likelihoods were used as weights of evidence in favour of each model (Akaike weights). As likelihood functions scale exponentially with the number of data points, with our data sets that typically contain 16,000–60,000 runs and 3,000–11,000 flights for each experimental condition, Akaike weights can approach 1 for the model that is dominantly favoured. This has allowed unambiguous selection of the more likely model.

**Numerical simulations.** We consider that a cargo is transported against a constant external opposing force  $F$  along a microtubule (Fig. 2) with  $\bar{n}$  motors

available for binding. At time  $t$ ,  $n$  ( $0 < n \leq \bar{n}$ ) motors are engaged, sharing the load  $F/n$ . The unbinding rate for engaged motors to dissociate from the microtubule is load-dependent,  $\varepsilon(n) = n\varepsilon_0 \exp(F/(nF_d))$ , where  $\varepsilon_0$  is the zero-load unbinding rate and  $F_d$  is the detachment force. The binding rate is  $\pi(n) = (\bar{n} - n)\pi_0$ , as it is limited by the number of available unbound motors ( $\bar{n} - n$ ), and  $\pi_0$  is the binding constant for a single motor.

The trajectories are generated by the Gillespie algorithm. Briefly, at  $t = 0$ ,  $\bar{n}$  is randomly selected from a discrete uniform distribution in the interval  $[1, N_{\text{max}}]$ , where  $N_{\text{max}}$  is the maximum number of motors that can be possibly available. This number should be physically bound by the maximum density of the motors attached to the cargo surface, and depends on the cargo size and the surface area that is close to the microtubule<sup>29</sup>. At each time step, with probability  $p = \pi(n)/(\varepsilon(n) + \pi(n))$ , an available motor may bind; otherwise, an engaged motor unbinds. Then time advances by a random number  $\delta t$  drawn from an exponential distribution function with a mean of  $1/(\varepsilon(n) + \pi(n))$ . If  $F/n > F_s$  ( $F_s$  is stall force), the cargo moves by  $v\delta t$ , assuming a constant velocity  $v$ ; if not, the transport pauses. If  $n$  drops to zero, a 'flight' ends, the transport turns with a random angle, and a new  $\bar{n}$  is assigned. A 'flight' also ends if the length exceeds the limit (100  $\mu\text{m}$ ) representing the size of a cell. We found that the numerical results are insensitive to the length limit used. This physical process generates numerically length-distribution functions, which have shapes determined by a set of dimensionless parameters,  $F/F_d$ ,  $\pi_0/\varepsilon_0$ ,  $F/F_s$ , and  $N_{\text{max}}$  (Supplementary Fig. 6). Among these parameters,  $F/F_s$  contributes only to the run length distribution without affecting the flight-length distribution. To compare with experiments, simulated trajectories are mapped to the experimental length scale by tuning the length unit,  $v/\varepsilon_0$  (Supplementary Table 1). One million flights were simulated for each parameter set.

Received 1 September 2013; accepted 2 February 2015;  
published online 30 March 2015

## References

- Shlesinger, M. F., Zaslavsky, G. M. & Klafter, J. Strange kinetics. *Nature* **363**, 31–37 (1993).
- Mantegna, R. N. & Stanley, H. E. Stochastic-process with ultraslow convergence to a Gaussian: The truncated Lévy flight. *Phys. Rev. Lett.* **73**, 2946–2949 (1994).
- Viswanathan, G. M. *et al.* Optimizing the success of random searches. *Nature* **401**, 911–914 (1999).
- Palyulin, V. V., Chechkin, A. V. & Metzler, R. Lévy flights do not always optimize random blind search for sparse targets. *Proc. Natl Acad. Sci. USA* **111**, 2931–2936 (2014).
- Bartumeus, F., Peters, F., Pueyo, S., Marrase, C. & Catalan, J. Helical Lévy walks: Adjusting searching statistics to resource availability in microzooplankton. *Proc. Natl Acad. Sci. USA* **100**, 12771–12775 (2003).
- Barthelemy, P., Bertolotti, J. & Wiersma, D. S. A Lévy flight for light. *Nature* **453**, 495–498 (2008).
- De Jager, M., Weissing, F. J., Herman, P. M. J., Nolet, B. A. & van de Koppel, J. Lévy walks evolve through interaction between movement and environmental complexity. *Science* **332**, 1551–1553 (2011).
- Harris, T. H. *et al.* Generalized Lévy walks and the role of chemokines in migration of effector CD8(+) T cells. *Nature* **486**, 545–549 (2012).
- Bao, G. & Suresh, S. Cell and molecular mechanics of biological materials. *Nature Mater.* **2**, 715–725 (2003).
- Loverdo, C., Benichou, O., Moreau, M. & Voituriez, R. Enhanced reaction kinetics in biological cells. *Nature Phys.* **4**, 134–137 (2008).
- Wang, B., Kuo, J. & Granick, S. Bursts of active transport in living cells. *Phys. Rev. Lett.* **111**, 208102 (2013).
- Trong, P. K., Guck, J. & Goldstein, R. E. Coupling of active motion and advection shapes intracellular cargo transport. *Phys. Rev. Lett.* **109**, 028104 (2012).
- Brangwynne, C. P., Koenderink, G. H., MacKintosh, F. C. & Weitz, D. A. Intracellular transport by active diffusion. *Trends Cell Biol.* **19**, 423–427 (2009).
- Tabi, S. M. A. *et al.* Intracellular transport of insulin granules is a subordinated random walk. *Proc. Natl Acad. Sci. USA* **110**, 4911–4916 (2013).
- Fakhri, N. *et al.* High-resolution mapping of intracellular fluctuations using carbon nanotubes. *Science* **344**, 1031–1035 (2014).
- Bouchaud, J. P. & Georges, A. Anomalous diffusion in disordered media: Statistical mechanisms, models and physical applications. *Phys. Rep.* **195**, 127–293 (1990).
- Peterson, J., Dixit, P. D. & Dill, K. A. A maximum entropy framework for nonexponential distributions. *Proc. Natl Acad. Sci. USA* **110**, 20380–20385 (2013).
- Huet, S. *et al.* Analysis of transient behavior in complex trajectories: Application to secretory vesicle dynamics. *Biophys. J.* **91**, 3542–3559 (2006).

19. Arcizet, D., Meier, B., Sackmann, E., Raedler, J. O. & Heinrich, D. Temporal analysis of active and passive transport in living cells. *Phys. Rev. Lett.* **101**, 248103 (2008).
20. Mueller, M. J. I., Klumpp, S. & Lipowsky, R. Tug-of-war as a cooperative mechanism for bidirectional cargo transport by molecular motors. *Proc. Natl Acad. Sci. USA* **105**, 4609–4614 (2008).
21. Klumpp, S. & Lipowsky, R. Cooperative cargo transport by several molecular motors. *Proc. Natl Acad. Sci. USA* **102**, 17284–17289 (2005).
22. Howard, J. Mechanical signaling in networks of motor and cytoskeletal proteins. *Annu. Rev. Biophys.* **38**, 217–234 (2009).
23. Bressloff, P. C. & Newby, J. M. Stochastic models of intracellular transport. *Rev. Mod. Phys.* **85**, 135–196 (2013).
24. Reilein, A., Yamada, S. & Nelson, W. J. Self-organization of an acentrosomal microtubule network at the basal cortex of polarized epithelial cells. *J. Cell Biol.* **171**, 845–855 (2005).
25. Chen, K., Wang, B., Guan, J. & Granick, S. Diagnosing heterogeneous dynamics in single-molecule/particle trajectories with multiscale wavelets. *ACS Nano* **7**, 8634–8644 (2013).
26. Balint, S., Verdeny Vilanova, I., Sandoval Alvarez, A. & Lakadamyali, M. Correlative live-cell and superresolution microscopy reveals cargo transport dynamics at microtubule intersections. *Proc. Natl Acad. Sci. USA* **110**, 3375–3380 (2013).
27. Ross, J. L., Ali, M. Y. & Warshaw, D. M. Cargo transport: Molecular motors navigate a complex cytoskeleton. *Curr. Opin. Cell Biol.* **20**, 41–47 (2008).
28. Edwards, A. M. *et al.* Revisiting Lévy flight search patterns of wandering albatrosses, bumblebees and deer. *Nature* **449**, 1044–1048 (2007).
29. Herold, C., Leduc, C., Stock, R., Diez, S. & Schwille, P. Long-range transport of giant vesicles along microtubule networks. *ChemPhysChem* **13**, 1001–1006 (2012).
30. Vergassola, M., Villermaux, E. & Shraiman, B. I. ‘Infotaxis’ as a strategy for searching without gradients. *Nature* **445**, 406–409 (2007).

### Acknowledgements

This work was supported by the US Department of Energy, Division of Materials Science, under Award DEFG02-02ER46019. B.W. holds a Career Award at the Scientific Interface from the Burroughs Wellcome Fund. S.G. acknowledges office support from the Institute for Basic Science, Project Code IBS-R020-D1. We thank J. Kuo and S. C. Bae for experimental help, and J. Cheng for cell culture lab space.

### Author contributions

K.C. and B.W. developed the analysis; B.W. designed and performed the experiment; K.C., B.W. and S.G. wrote the paper.

### Additional information

Supplementary information is available in the [online version of the paper](#). Reprints and permissions information is available online at [www.nature.com/reprints](http://www.nature.com/reprints). Correspondence and requests for materials should be addressed to B.W. or S.G.

### Competing financial interests

The authors declare no competing financial interests.